JACS
JOURNAL OF THE AMERICAN CHEMICAL SOCIETY

Communication

pubs.acs.org/JACS

Designed Catalysts from Pt Nanoparticles Supported on Macroporous Oxides for Selective Isomerization of *n*-Hexane

Kwangjin An, Selim Alayoglu, Nathan Musselwhite, Kyungsu Na, and Gabor A. Somorjai*

Department of Chemistry, University of California, Berkeley, California 94720, United States

Chemical Sciences Division and Materials Sciences Division, Lawrence Berkeley National Laboratory, Berkeley, California 94720, United States

Supporting Information

ABSTRACT: Selective isomerization toward branched hydrocarbons is an important catalytic process in oil refining to obtain high-octane gasoline with minimal content of aromatic compounds. Colloidal Pt nanoparticles with controlled sizes of 1.7, 2.7, and 5.5 nm were deposited onto ordered macroporous oxides of SiO_2, Al_2O_3, TiO_2, Nb_2O_5, Ta_2O_5, and ZrO_2 to investigate Pt size- and support-dependent catalytic selectivity in *n*-hexane isomerization. Among the macroporous oxides, Nb_2O_5 and Ta_2O_5 exhibited the highest product selectivity, yielding predominantly branched C_6 isomers, including 2- or 3-methylpentane, as desired products of *n*-hexane isomerization (140 Torr *n*-hexane and 620 Torr H_2 at 360 °C). *In situ* characterizations including X-ray diffraction and ambient-pressure X-ray photoelectron spectroscopy showed that the crystal structures of the oxides in Pt/oxide catalysts were not changed during the reaction and oxidation states of Nb_2O_5 were maintained under both H_2 and O_2 conditions. Fourier transform infrared spectra of pyridine adsorbed on the oxides showed that Lewis sites were the dominant acidic site of the oxides. Macroporous Nb_2O_5 and Ta_2O_5 were identified to play key roles in the selective isomerization by charge transfer at Pt−oxide interfaces. The selectivity was revealed to be Pt size-dependent, with improved isomer production as Pt sizes increased from 1.7 to 5.5 nm. When 5.5 nm Pt nanoparticles were supported on Nb_2O_5 or Ta_2O_5, the selectivity toward branched C_6 isomers was further increased, reaching ca. 97% with a minimum content of benzene, due to the combined effects of the Pt size and the strong metal−support interaction.

In the 21st century, catalysis aims for 100% selectivity, in order to realize "green chemistry", or the production of only one desired product at a high turnover rate without byproducts in multipath reactions.[1,2] Recent advances in colloidal chemistry provide a novel method to generate metal nanoparticles with precisely controlled size and shape, as well as porous materials used as supports with a high surface area and an ordered pore structure.[3] Since heterogeneous catalysts are prepared mainly by deposition of nanoparticles on oxide supports, oxide−metal interfaces have attracted much attention as important catalytic sites, along with the morphologies of metal nanoparticles and oxide supports.[4,5] Recent studies demonstrate that oxide−metal interfaces are responsible for changes in the catalytic activity and selectivity due to charge transfer between the metal and the oxide support.[6]

Catalytic reforming of hydrocarbons is of key importance for the production of high-octane gasoline in petroleum chemistry.[7] Since environmental regulations limit aromatic compounds in gasoline due to their carcinogenic nature, selective production of branched hydrocarbons with high octane number is highly desirable. *n*-Hexane isomerization is an excellent model reaction to study structure- and support-dependent catalytic selectivity, because it has four distinct reaction pathways: isomerization, cyclization, aromatization, and cracking.[7] Previous studies revealed the possibility of changing catalytic selectivity by introducing different oxide supports to the transition metal catalyst as well as by manipulating the size and shape of metal nanoparticles.[6,8] Recently, several mesoporous oxides were used for the preparation of Pt nanoparticle-supported catalysts to study the effect of the support in catalytic hydrogenation reactions.[9,10] However, the small pore sizes (less than 3 nm) of several oxides limited their incorporation of metal nanoparticles with various sizes (1.5−5.0 nm), resulting in metal loading less than 0.1 wt%.[9]

Herein, macroporous oxides were synthesized by using polymer microspheres as a hard template, generating highly crystalline Al_2O_3, TiO_2, Nb_2O_5, Ta_2O_5, and ZrO_2 with an average pore size of ∼300 nm. Colloidal Pt nanoparticles with sizes of 1.7, 2.7, and 5.5 nm were deposited onto them to investigate the Pt size- and support-dependent catalytic selectivity and their reaction mechanism in *n*-hexane isomerization. By applying Pt nanoparticles with controlled sizes onto different types of supports, reaction pathways could be changed by combining the effects of the Pt metal and the metal−support interaction. From this study, the best catalyst could be designed for the selective production of branched isomers with high octane numbers and the minimal concentration of benzene.

While synthetic methods for mesoporous silicas such as MCM-41, SBA-15, and MCF-17 are well-established to manipulate their pore structures,[11] preparation of non-siliceous oxides with large pore sizes (>20 nm) has remained challenging for effective loading of nanoparticles with various sizes. The hard-templating approach using polystyrene beads was chosen to synthesize highly crystalline macroporous oxides of Al_2O_3, TiO_2, Nb_2O_5, Ta_2O_5, and ZrO_2 with a pore size greater than

Received: February 25, 2014
Published: April 28, 2014

   dx.doi.org/10.1021/ja5018656 | *J. Am. Chem. Soc.* 2014, 136, 6830−6833

300 nm.[12,13] Figure 1a shows a general procedure for the preparation of macroporous oxides and their supported Pt nanoparticle catalysts.

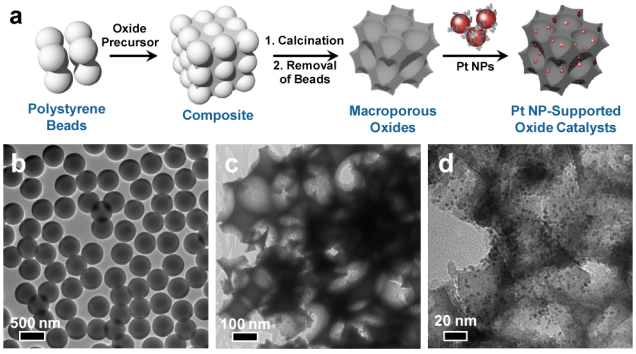

Figure 1. (a) Illustration of the preparation of macroporous oxides using the polymer template and their supported Pt nanoparticle catalysts. (b–d) TEM images of polystyrene beads as a template (b), the resulting Al_2O_3 replicas with macropores (c), and 2.7 nm Pt nanoparticle-supported macroporous Al_2O_3 catalysts (d).

Transmission electron microscopy (TEM) images of macroporous oxides demonstrate that macro- and mesopores of the oxide replicas resulted from the polystyrene beads and P123 surfactants,[13] respectively (Figure 1b,c). During the calcinations at 700 °C, polystyrene beads with a diameter of 500 nm were shrunk and removed completely to generate 300 nm macropores, and the creation of crystalline walls was confirmed by X-ray diffraction (XRD) patterns (Figures S1 and S2). The sizes of mesopores generated by P123 were 3–11 nm, obtained from the adsorption branch using the BJH algorithm. The BET surface areas of the resulting oxides were ca. 100 m^2/g for Al_2O_3, Nb_2O_5, and Ta_2O_5, while TiO_2 and ZrO_2 had relatively small areas (Table S1) due to their large grain sizes. The dual pores of the oxides enabled effective loading of poly(vinylpyrrolidone) (PVP)-capped Pt nanoparticles, as shown in Figure 1d. In our previous study, mesoporous Ta_2O_5 could not be loaded with 1.9 nm Pt nanoparticles homogeneously (less than 0.05 wt% Pt) due to its small pores (ca. 2.7 nm).[9] The polymer templating strategy enabled us to incorporate PVP-capped Pt nanoparticles into macroporous oxides up to 1 wt%, regardless of the nanoparticle size.

n-Hexane isomerization as a multipath reaction was carried out over 2.7 nm Pt nanoparticles on different kinds of oxide supports over the temperature range of 240–360 °C in 140 Torr *n*-hexane and 620 Torr H_2 (Table S2). Under these reaction conditions, multiple products were generated through four distinct reaction pathways: branched isomers via isomerization, methylcyclopentane and cyclohexane via cyclization, benzene via dehydrogenation of cyclohexane (aromatization), and cracked hydrocarbons with short chains (C_1–C_5 paraffin) via hydrogenolysis (Figure 2a). As shown in Figure 2b, branched C_6 isomers including 2- or 3-methylpentane and 2,2- or 2,3-dimethylbutane, which are desirable for the production of high-octane gasoline, were generated as major products with greater than 45% selectivity over Pt/SiO_2 and Pt/Al_2O_3 catalysts. Methylcyclopentane, C_1–C_5 alkanes, and benzene were produced in with progressively lower selectivities. While the silica support does not contribute to the catalytic activity of Pt,[14] it is noteworthy that the macroporous alumina with an acidic site showed a negligible effect of the support in this study. When macroporous TiO_2, Nb_2O_5, Ta_2O_5, and ZrO_2 were used as oxide supports, the product selectivity was significantly changed (Figure 2b, Table S2). When 2.7 nm Pt nanoparticles were supported on TiO_2, Nb_2O_5, and Ta_2O_5, the amount of C_6 isomers formed was increased at the expense of other products at 360 °C.

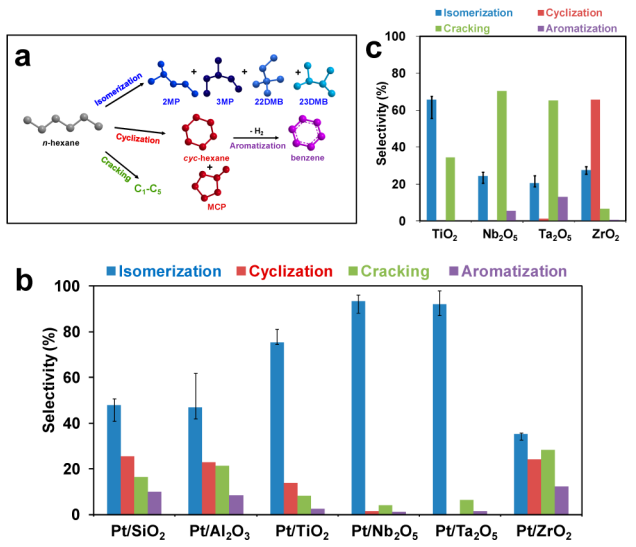

Figure 2. (a) Reaction pathways and possible products of *n*-hexane isomerization. (b,c) Product selectivity over 2.7 nm Pt nanoparticle catalysts supported on different kinds of oxide supports (b) and pure macroporous oxides (c) at 360 °C. The reaction was conducted with a hexane:H_2 ratio of 1:4.3 at temperatures ranging from 240 to 360 °C at ambient pressure.

When the reaction was conducted over macroporous oxides without Pt loading (Figure 2c), pure macroporous Nb_2O_5 and Ta_2O_5 yielded cracking products predominantly, but the conversion was 10-fold lower compared to those obtained on Pt-supported catalysts. In the case of pure SiO_2 and Al_2O_3, no catalytic activity was found in the current reaction at 360 °C, while the other oxides were catalytically active. It is noteworthy that Rh and Ir, which are used as promoters in the industrial catalyst, exhibited the same results with Nb_2O_5 and Ta_2O_5, yielding cracking products dominantly in the reaction. When the reaction was carried out over monometallic Rh (6.5 nm) and Ir (1.5 nm) nanoparticles under identical reaction condition, Rh and Ir nanoparticles favored the cracking pathway with 90% selectivity.[15] Oxides of group V metals such as Nb and Ta have been investigated for their catalytic properties, because they possess variable oxidation states, an acidic surface, and an empty d-orbital which allow electron transfer between the reactants and surface active site during the reaction.[16,17]

We characterized Pt/oxide catalysts using XRD and ambient-pressure X-ray photoelectron spectroscopy (APXPS) under catalytically relevant reaction conditions. *In situ* XRD study of Pt/Ta_2O_5 and Pt/ZrO_2 in 150 Torr H_2 at 360 °C confirmed no structural changes under the reaction conditions (Figure S3). APXPS identified the presence of various oxidation states in oxides under H_2 or O_2 at 360 °C. While Pt/TiO_2 showed a reduced charge state of TiO_2 under H_2 atmosphere, Pt/Nb_2O_5 had identical XP spectra in both H_2 and O_2 environments (Figures S4 and S5). Furthermore, there is no measurable XPS signature of charge transfer between metallic Pt and the metal oxides (Figure S6). Therefore, the stable charge state was

dx.doi.org/10.1021/ja5018656 | J. Am. Chem. Soc. 2014, 136, 6830–6833

responsible for the enhanced isomerization selectivity of the Nb_2O_5 support beyond the TiO_2 support. This means that such a charge transfer is fast, and the reduced charge centers are short-lived in the time scale of our XPS measurements. TiO_2, Nb_2O_5, and Ta_2O_5 are known as acidic oxides exhibiting a strong metal−support interaction (SMSI) effect. Boffa et al. reported that TiO_2, Nb_2O_5, and Ta_2O_5 showed the greatest promotional effect in CO and CO_2 hydrogenation by SMSI at the interfaces of the oxides and Rh foils.[8a] They found that oxides with higher oxidation states increased the reaction rate by changing Lewis acidity. We also carried out Fourier transform infrared (FT-IR) spectroscopy to indentify surface acidic sites on the oxides. FT-IR spectra of pyridine adsorbed on the oxides show that Al_2O_3, TiO_2, Nb_2O_5, Ta_2O_5, and ZrO_2 have characteristic peaks typical of Lewis and Brönsted acidic sites and H-bonded pyridine, and their acidic properties mostly come from Lewis acidic sites (Figure S7). From these results, we concluded that Nb_2O_5 and Ta_2O_5, with stable oxidation states of 5+, promoted the highest selectivity for isomerization. TiO_2 was the next due to its oxidation state less than 4+ (Figure S4).

With a typical bifunctional reforming catalyst, dehydrogenation/hydrogenation occurs on the Pt metal, while isomerization is determined by the oxide support.[7,18] Schmal and coworkers also reported the promoting effect of Nb_2O_5-supported Pt catalysts, resulting in the selectivity change in hydrocarbon hydrogenation.[19,20] They found that the production of light hydrocarbons was decreased at the expense of C7 isomers and alkenes over Pt/Nb_2O_5 in *n*-heptane dehydrogenation by the SMSI effect, when compared to the reaction on Pt/Al_2O_3.[19] The selectivity change on Pt/Nb_2O_5 due to SMSI was also confirmed in 1,3-butadiene hydrogenation.[20] In those reports, the increase in the electron density of Pt on Pt/Nb_2O_5 was responsible for the SMSI effect and the subsequent selectivity change. Therefore, we concluded that the acidic Nb_2O_5 and Ta_2O_5 facilitated electron transfer to Pt nanoparticles with the formation of higher electron density, leading to selective isomerization.

PVP organic capping molecules protect the surface of Pt nanoparticles during the reaction. When the PVP was substantially removed following calcination at 360 °C in air, it enabled a direct contact between the Pt and the oxide during the reaction. To study the role of the oxide−metal interface, we conducted the reaction over Pt/Nb_2O_5 and Pt/Ta_2O_5, where the catalysts were prepared separately before and after removal of the PVP. Without calcination, Pt/Nb_2O_5 and Pt/Ta_2O_5 catalysts, with a poor contact between the Pt and the oxide, exhibited selectivity trends similar to those of Pt/SiO_2 or Pt/Al_2O_3 in the reaction (Figure S8). However, over Pt/Nb_2O_5 and Pt/Ta_2O_5 catalysts from which the PVP was removed by calcination, the catalytic selectivity toward isomers was enhanced, as discussed above. It is concluded that the oxide−metal interface acts to change catalytic selectivity, promoting selective isomerization.

Previous studies on reforming of C_6 hydrocarbons over supported Pt nanoparticle catalysts have shown that isomerization was enhanced at increased Pt sizes.[21,22] In the current study, uniformly synthesized Pt nanoparticles with sizes ranging from 1.7 to 5.5 nm were supported on macroporous aluminas and utilized in *n*-hexane isomerization. As shown in Figure 3, as the size of Pt was increased, the selectivity toward isomers was also increased, in agreement with the observations with Pt-supported mesoporous silicas in the previous studies.[21,22] It is

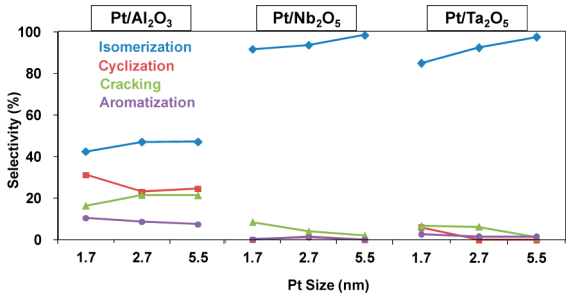

Figure 3. Pt size- and support-dependent catalytic selectivity in *n*-hexane isomerization at 360 °C. Pt nanoparticles of 1.7, 2.7, and 5.5 nm were supported on macroporous Al_2O_3, Nb_2O_5, and Ta_2O_5, respectively.

known that large Pt nanoparticles (at and above 5 nm) have a larger concentration of terrace sites than smaller sizes (1.5−3 nm), which dominantly contain corner or edge sites.[21] In reaction studies on *n*-hexane isomerization over Pt single crystals, Pt (100) or (111) surfaces were shown to yield increased isomer products due to their well-defined terrace sites.[7b]

Activation energies measured from this reaction over different Pt particle sizes, oxide support catalysts, and even single-crystal Pt catalysts have similar values (26−28 kcal/mol),[7b] demonstrating that the isomerization of *n*-hexane follows the same mechanism regardless of carbon poisoning from capping agents or other sources.

XPS images of Pt-supported oxide catalysts in 100 mTorr H_2 at 360 °C revealed a Pt:C ratio of 1:3, exhibiting the presence of carbons related or unrelated to PVP on the Pt surface (Figure S9). Although the wispy PVP caused inevitable sintering during the calcination and catalytic reaction, the current reaction conditions (up to 360 °C) seemed to be sufficient to conclude that there exist Pt size-dependent catalytic properties, because the initial order of size distributions was maintained after the reaction (Figure S10). With the knowledge that large Pt nanoparticles yielded higher selectivity toward isomerization due to their abundant terrace sites, we loaded Pt nanoparticles of three different sizes onto macroporous Nb_2O_5 and Ta_2O_5 in order to determine the best catalyst for the isomerization reaction. In terms of turnover frequencies (TOFs), the smaller Pt nanoparticles had higher TOFs (Figure S11). Nevertheless, it was concluded that 5.5 nm Pt nanoparticles supported on Nb_2O_5 or Ta_2O_5 yielded the best catalyst, giving ca. 97% selectivity toward the desired isomer products, as shown in Figure 3.

In summary, rational combination of metal nanoparticles and oxide supports can increase catalytic selectivity to obtain only desirable products, because metal, oxide support, and the oxide−metal interface simultaneously influence the catalytic performance. In the isomerization of *n*-hexane over Pt nanoparticle-supported catalysts, when macroporous Nb_2O_5 and Ta_2O_5 were used as supports, the production of C_6 isomers as the most desired products was increased selectively, due to the effect of SMSI. The Nb_2O_5 and Ta_2O_5 allowed charge transfer at the Pt−oxide interfaces and thus high electron density of the Pt during the reaction. While Pt nanoparticles showed size-dependent selectivity, large-sized Pt nanoparticles (5.5 nm) supported on Nb_2O_5 or Ta_2O_5 produced branched hydrocarbons with ca. 97% selectivity. By utilizing colloidal synthetic chemistry, a selective catalyst

dx.doi.org/10.1021/ja5018656 | J. Am. Chem. Soc. 2014, 136, 6830−6833

composed of well-defined metal nanoparticles and oxide supports can be designed appositely to realize 100% selectivity without any undesired byproducts.

■ ASSOCIATED CONTENT

Supporting Information

Experiment details; TEM, XRD, and nitrogen adsorption−desorption isotherms of macroporous oxides and their Pt-supported catalysts (Figures S1−S3 and Table S1); APXPS and FT-IR spectra of Pt/oxide catalysts (Figures S4−S7 and S9); catalytic activity and selectivity details for *n*-hexane isomerization (Table S2 and Figures S8 and S11); and Pt size distribution histograms of the supported catalysts (Figures S10); This material is available free of charge via the Internet at http://pubs.acs.org.

■ AUTHOR INFORMATION

Corresponding Author

somorjai@berkeley.edu

Notes

The authors declare no competing financial interest.

■ ACKNOWLEDGMENTS

This work was supported the Director, Office of Basic Energy Sciences, Materials Sciences and Engineering Division, U.S. Department of Energy, under Contract DE-AC02-05CH11231. The user project at the Advanced Light Source and the Molecular Foundry at the Lawrence Berkeley National Laboratory was also supported by the Director, Office of Science, Office of Basic Energy Sciences, U.S. Department of Energy, under Contract DE-AC02-05CH11231. The nanoparticle synthesis was funded by Chevron Corporation. We thank Profs. A. Paul Alivisatos, Peidong Yang, and Omar Yaghi for use of the TEM and XRD instruments; Dr. Gérôme Melaet, Walter Ralston, and Stephanus Axnanda for helps in APXPS measurements; Jae-Youn Shin for helping with material preparation; and Jae Hyuck Yoo for the scheme in Figure 1.

■ REFERENCES

(1) Geus, J. W.; van Ween, J. A. R. In *Catalysis: An Integrated Approach to Homogeneous, Heterogeneous and Industrial Catalysis*; Moulijn, J. A., van Leeuwen, P. W. N. M., van Santen, R. A., Eds.; Elsevier: Amsterdam, 1993.

(2) (a) Somorjai, G. A. *Introduction to Surface Chemistry and Catalysis*; Wiley: New York, 1994. (b) Somorjai, G. A.; Park, J. Y. *Angew. Chem., Int. Ed.* **2008**, *47*, 9212.

(3) An, K.; Somorjai, G. A. *ChemCatChem* **2012**, *4*, 1512.

(4) Tauster, S. J.; Fung, S. C.; Garten, R. L. *J. Am. Chem. Soc.* **1978**, *100*, 170.

(5) Wang, S. Y.; Moon, S. H.; Vannice, M. A. *J. Catal.* **1981**, *71*, 167.

(6) Gross, E.; Somorjai, G. A. *Top Catal* **2013**, *56*, 1049.

(7) (a) Hagen, J. *Industrial Catalysis: A Practical Approach*, 2nd ed.; Wiley-VCH: Weinheim, 2006. (b) Davis, S. M.; Zaera, F.; Somorjai, G. A. *J. Catal.* **1984**, *85*, 206. (c) Ciapetta, F. G.; Hunter, J. B. *Ind. Eng. Chem.* **1953**, *45*, 147.

(8) (a) Boffa, A. B.; Lin, C.; Bell, A. T.; Somorjai, G. A. *Catal. Lett.* **1994**, *27*, 243. (b) Baker, L. R.; Kennedy, G.; Van Spronsen, M.; Hervier, A.; Cai, X. J.; Chen, S. Y.; Wang, L. W.; Somorjai, G. A. *J. Am. Chem. Soc.* **2012**, *134*, 14208.

(9) An, K.; Musselwhite, N.; Kennedy, G.; Pushkarev, V. V.; Baker, L. R.; Somorjai, G. A. *J. Colloid Interface Sci.* **2013**, *392*, 122.

(10) Rao, Y. X.; Antonelli, D. M. *J. Mater. Chem.* **2009**, *19*, 1937.

(11) Wan, Y.; Zhao, D. Y. *Chem. Rev.* **2007**, *107*, 2821.

(12) (a) Holland, B. T.; Blanford, C. F.; Stein, A. *Science* **1998**, *281*, 538. (b) Stein, A. *Microporous Mesoporous Mater.* **2001**, *44*, 227.

(13) Dacquin, J. P.; Dhainaut, J.; Duprez, D.; Royer, S.; Lee, A. F.; Wilson, K. *J. Am. Chem. Soc.* **2009**, *131*, 12896.

(14) An, K.; Alayoglu, S.; Musselwhite, N.; Plamthottam, S.; Melaet, G.; Lindeman, A. E.; Somorjai, G. A. *J. Am. Chem. Soc.* **2013**, *135*, 16689.

(15) Musselwhite, N.; Alayoglu, S.; Melaet, G.; Pushkarev, V. V.; Lindeman, A. E.; An, K.; Somorjai, G. A. *Catal. Lett.* **2013**, *143*, 907.

(16) (a) Rao, Y. X.; Kang, J. J.; Antonelli, D. *J. Am. Chem. Soc.* **2008**, *130*, 394. (b) Rao, Y. X.; Kang, J. J.; Trudeau, M.; Antonelli, D. M. *J. Catal.* **2009**, *266*, 1. (c) Yue, C.; Michel, T.; Antonelli, D. *Chem. Commun.* **2006**, 1918. (d) Borgschulte, A.; Rector, J. H.; Dam, B.; Griessen, R.; Zuttel, A. *J. Catal.* **2005**, *235*, 353.

(17) Yue, C.; Michel, T.; Antonelli, D. *Chem. Commun.* **2006**, 1918.

(18) Davis, R. J.; Derouane, E. G. *Nature* **1991**, *349*, 313.

(19) Schmal, M.; Aranda, D. A. G.; Soares, R. R.; Noronha, F. B.; Frydman, A. *Catal. Today* **2000**, *57*, 169.

(20) Aranda, D. A. G.; Schmal, M. *J. Catal.* **1997**, *171*, 398.

(21) Alayoglu, S.; Pushkarev, V. V.; Musselwhite, N.; An, K.; Beaumont, S. K.; Somorjai, G. A. *Top. Catal.* **2012**, *55*, 723.

(22) (a) Boudart, M.; Aldag, A. W.; Ptak, L. D.; Benson, J. E. *J. Catal.* **1968**, *11*, 35. (b) Botman, M. J. P.; Devreugd, K.; Zandbergen, H. W.; Deblock, R.; Ponec, V. *J. Catal.* **1989**, *116*, 467. (c) Foger, K.; Anderson, J. R. *J. Catal.* **1978**, *54*, 318.